Journal of Hazardous Materials Advances 22 (2026) 101168

Contents lists available at ScienceDirect

Journal of Hazardous Materials Advances

journal homepage: www.elsevier.com/locate/hazadv

NIR–SWIR hyperspectral imaging of powder released from simulated weathering of NOA-bearing serpentinites: a pilot investigation on serpentinites from Tuscany (Italy)

Lorenzo Marzini [a,*], Daniele Ciofini [a], Juri Agresti [a], Andrea Azelio Mencaglia [a], Leonardo Disperati [b], Narcisa Mihaela Marian [b], Nadia Valletti [b], Cecilia Viti [b], Sergio Bellagamba [c], Sergio Malinconico [c], Federica Paglietti [c], Salvatore Siano [a], Iacopo Osticioli [a]

[a] Istituto di Fisica Applicata "N. Carrara" - Consiglio Nazionale delle Ricerche (IFAC-CNR), Florence, Italy
[b] Department of Physical Sciences, Earth and Environment (DSFTA) of University of Siena, Siena, Italy
[c] Italian Workers Compensation Authority (INAIL), Department of Technological Innovations and Safety of Plants, Products and Anthropic Settlements, Rome, Italy

ARTICLE INFO

Keywords:
Serpentinites
Weathering
Slake Durability Test
Asbestos
NOA
Hyperspectral imaging
Chrysotile
NIR-SWIR

ABSTRACT

Natural weathering processes, environmental cycles and anthropogenic activities (mining, excavation, road construction) involving naturally occurring asbestos (NOA) materials pose environmental and human health issues due to the potential release of pathogenic fibers. This pilot investigation focuses on the Slake Durability Test (SDT) to simulate weathering cycles and assess the long-term slaking behaviour of serpentinite samples from Elba Island and the province of Siena (Tuscany, Italy), lithologies commonly hosting asbestos minerals. The resulting rock powders from the SDT were analysed using a novel portable NIR-SWIR hyperspectral scan imaging tool, enabling rapid detection and mapping of serpentine minerals through their characteristic spectral features. To validate this results, traditional and complementary FTIR and SEM analyses were performed. This novel approach, combining laboratory engineering-geological analysis and fast NIR-SWIR hyperspectral imaging (HSI) techniques, provided new insights on the durability and the hazard potential (in terms of release index) of serpentinites, while reducing the costs and time-consuming issues of conventional laboratory methods.

1. Introduction

Serpentinites represent the most common lithologies hosting asbestos minerals (Mevel, 2003; Vignaroli et al., 2011), which are known to cause serious health hazards (Curado et al., 2024). These lithologies are hydrated mafic and ultramafic rocks deriving from the hydration of peridotites (Bonatti and Michael, 1989; O'Hanley, 1996) and are the main components of the so-called group of Naturally Occurring Asbestos (NOA). Serpentinite rocks represent a valuable natural resource since they can form important ore deposits of several metals, such as chromium, nickel, or cobalt, either as lateritic deposits or sulphides or even talc (Haldar, 2020). Examples of the use of such rocks as ornamental stones (the so-called "green marble" or "green stones") can be found in cladding, flooring or architectonical elements of historical and modern buildings all around the world (Carmignano and Brandao, 2023). This widespread use of NOA materials represent a relevant health risk due to the potential release of asbestos fibres in the environment during their extraction and processing (sawing, drilling, polishing), as well as due to a variety of physical, chemical and biological weathering processes that can produce health hazardous powders (Harper, 2008; Malinconico et al., 2022).

The identification and quantification of asbestos fibers that can be released by decorative serpentinite stone elements is crucial to evaluate specific toxicities, disposal protocols, and to plan preventive measures and strategies (Marzini et al., 2024; Bellagamba et al., 2024). Along the last decades significant efforts have been dedicated to the characterization of NOA and ACM (Asbestos Containing Materials) samples using laboratory analytical approaches (e.g. X-ray diffraction (XRD)), thermal analysis, Fourier transform infrared spectroscopy (FTIR), and scanning electron microscopy (SEM-EDX)) (Cossio et al., 2018; Punturo et al.,

* Corresponding author at: Nello Carrara Institute of Applied Physics National Research Council, Italy.
E-mail address: l.marzini@ifac.cnr.it (L. Marzini).

https://doi.org/10.1016/j.hazadv.2026.101168
Received 3 February 2026; Received in revised form 27 March 2026; Accepted 11 April 2026
Available online 12 April 2026

2019; Rivero Crespo et al., 2019; Zholobenko et al., 2021). These traditional laboratory-based techniques require sample preparations and complex analytical routines (Malinconico et al., 2022), they are expensive and not satisfactorily suited for characterization problems requiring many analyses and chemometric methods. To overcome these limitations, in the last years significant efforts have been made in developing efficient portable instruments allowing for rapidly characterizing samples in situ using portable Raman, XRF, and IR spectroscopic techniques (Bloise and Miriello, 2018; Petriglieri et al., 2020; Bloise and Miriello, 2022; Marzini et al., 2025).Despite the advances offered by the mentioned techniques (essentially providing fast and in situ operability), a significant gap remains in the analytical workflow for assessing the hazard potential of NOA-bearing materials. Indeed, spectroscopy techniques such as Raman, XRF and FTIR are effective for pointwise identification of mineral phases but are inherently limited when analysing heterogeneous materials resulting from rock weathering and degradation phenomena, that requires higher spatial resolutions and mapping. Furthermore, standard protocols for quantitatively evaluating rock durability, such as the Slake Durability Test (SDT), produce fine-grained powders whose characterization still relies on time consuming laboratory analyses such as calibrated FTIR, whereas Raman is not suited for quantitative evaluations and standalone XRF data can hardly be interpreted in terms of phase contents.

Along with the development of portable spectroscopic instrumentations, hyperspectral imaging (HSI) has emerged as a powerful tool for asbestos detection due to the capacity of combine spatial coordinates of the image pixels (x,y) and the corresponding spectrum, I(λ), constituting the data cube, allowing for spatial characterization of heterogeneous samples without sample manipulation and/or alteration phases (Bonifazi et al., 2018). HSI applications towards asbestos detection have mainly focused on two different spatial scales: remote sensing for large area mapping and field-based material characterization. Focusing on the first approach, airborne and satellite hyperspectral platforms have been successfully used to identify asbestos-cement rooftops in urban and industrial areas using different computational approaches, ranging from spectral similarity metrics to machine learning techniques (Valdelamar Martínez et al., 2024). HSI remote sensing applications are primarily involved on the realization and updating of inventories related to land use planning and risk assessment of ACM present into the industrial and urban areas (Saba et al., 2026). Although remote sensing HSI data generally offer fast and reliable classification accuracy for large areas, they present significant logistical and economic limitations due to the fact that they require airborne surveys, with connected significant efforts. Focusing on field scale, HSI techniques have been applied to discriminate asbestos fibers in several materials, such as Construction and Demolition Waste (CDW) and soils (Bonifazi et al., 2019, 2022). This approach usually involves portable Short-Wave Infrared sensors (SWIR, from 1000 to 2500 nm) combined with chemometric analysis such as Hierarchical Partial Least Squares–Discriminant Analysis and Spectral Angle Mapper (SAM), allowing to obtain rapid acquisition of asbestos maps related to a large quantity of samples with a higher spatial resolution and without sample manipulation (Bonifazi et al., 2019; Marzini et al., 2025).

Due to the asbestos toxicological issues mentioned above, serpentinites should be characterized not only in terms of traditional petrographic and/or spectroscopic analysis, but also in terms of resistance against mechanical factors and stability related to alternation of wetting and drying conditions (the so-called rock durability feature) (Danaei and Fereidooni, 2023). Indeed, rocks that are sensitive to weakening effects will develop degradation phenomena when in contact with water (Bauer et al., 1981; Vergara and Triantafyllidis, 2016; Wong et al., 2016) and will reduce the uniaxial compressive strength (UCS) (Wong et al., 2016). Moreover, also temperature plays a relevant role and contribute to rock decay due to the development of internal stresses and cracks, which in turn facilitate water penetration (Hu et al., 2017), resulting in a cascade effect.

Both degradation effects of rocks induced by water and temperature variations can be evaluated for serpentinites using several methods of engineering geology (e.g., jar slake test, static slaking immersion test, slake index test, slake durability test-SDT) (Franklin and Chandra, 1972; Sadisun et al., 2002; Selen et al., 2020). Among these, SDT is a widely used test (Selen et al., 2020). It simulates weathering processes to assess durability resistance through mechanical shaking cycles of the rock within the test cylinder filled with water (Selen et al., 2020). Powder produced by repeated impacts among rock fragments in one or more weathering cycles can provide information on the release of the various mineral components of the rock itself.

This work presents the results of SDTs aimed at determining the amount and composition of slaking and disintegration of serpentinite rocks. According to the recommendation of the International Society for Rock Mechanics and Rock Engineering (ISRM, 1979) the Slake Durability Index (SDI) has been used for the overall quantification of the material losses. SDI is usually defined as the percentage ratio of the final to initial dry sample masses after two standard cycles of wetting and drying after the SDT, which were extended here to four cycles in order to simulate the long-term slaking behaviour of the selected serpentinite samples. For compositional characterization of the material, an innovative portable NIR-SWIR hyperspectral imaging (HSI) device was experimented to rapidly recognise, map and semi-quantify serpentine minerals released in weathering simulation cycles. The results achieved appear very promising to speed up the evaluation phase of SDT thus avoiding time-consuming and costly traditional laboratory analyses. To date, few studies were reported on the durability and related release index of serpentinites (Marzini et al., 2024; Selen et al., 2020). In these studies, such data were obtained through the combination of several approaches, including grinding tests, FTIR spectroscopy and the calibration curve method following the Italian legislation Decrees 14/5/96 and 152/2006 (Accardo et al., 2014; Marzini et al., 2024). Differently, the present pilot investigation implements SDT and NIR-SWIR HSI imaging methods providing a reliable pilot dataset of the serpentinite durability properties and the related powder characterization. Results provide preliminary useful information on the NOA response towards weathering phenomena. Further insights will be dedicated to the extension of the SDT and NIR-SWIR HSI analytical procedure to other serpentinites lithotypes with different fabrics and metamorphic grades.

2. Materials and methods

2.1. Analytical workflow

Fig. 1 summarizes the whole analytical procedure adopted in this pilot investigation. The workflow was characterized by two main analytical steps: the first consisted of a simulation of weathering processes using the SDT. The second involved the mapping and semi-quantification of NOA powder produced during the weathering simulation using a portable whisk broom NIR-SWIR hyperspectral imaging tool. The serpentinite samples were subjected to a first weathering simulation (wetting and drying cycles) ("SDT phase 1″) producing rock fragments and powder. Serpentine powders were characterised by using NIR-SWIR HSI (NIR-SWIR phase 1) as well as Scanning Electron Microscopy (SEM) and Diffuse Reflectance Infrared Fourier Transformed (DRIFT) analysis for comparison. Rock fragments underwent a new weathering process ("SDT phase 2") as well as another cycle of analysis (NIR-SWIR phase 2). The assessment of the evolution of serpentine contents (within rock powder) after n weathering process simulations was the final goal of the present analytical approach. All the steps of the analysis procedure, such as the selection of the samples, rock fragments preparation, and wetting and drying phases, were carried out using adequate protection devices towards the exposure to asbestos fibers. More details are provided in the following sections.

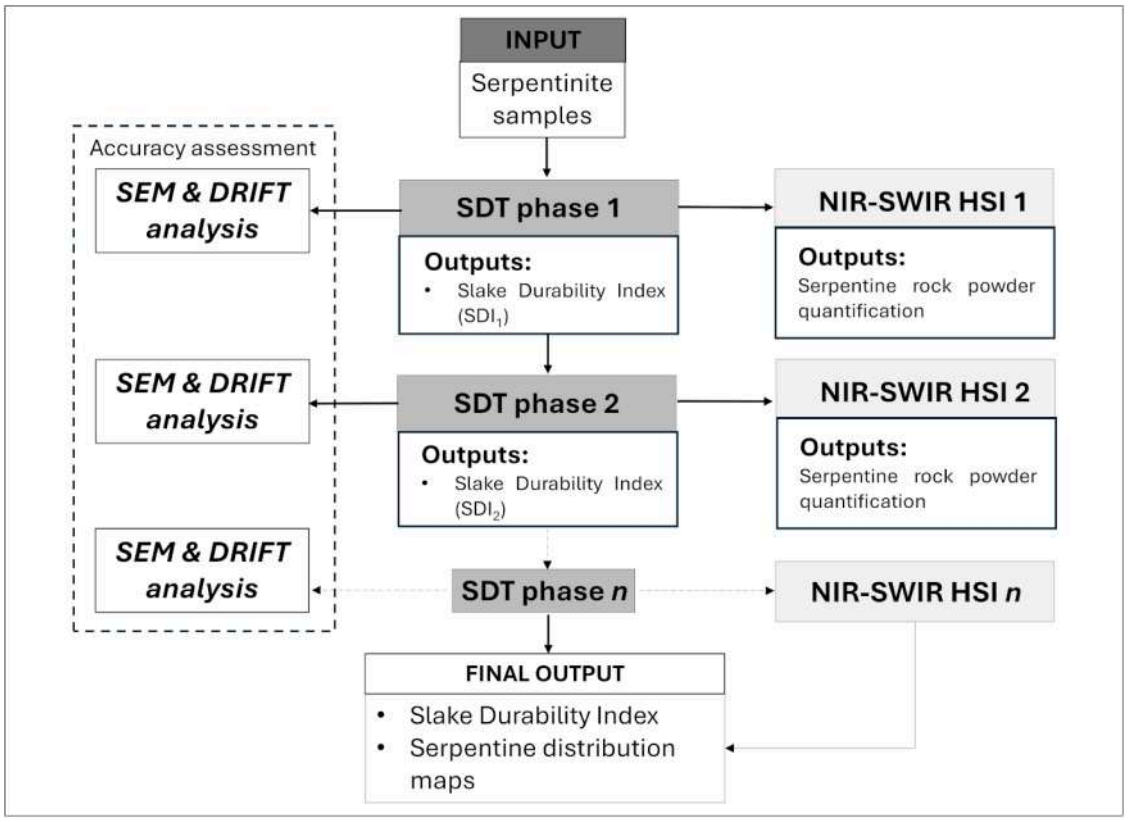

Fig. 1. Workflow diagram summarising the analytical protocol steps (SDT and NIR-SWIR), SEM, DRIFT analysis and related outputs (see text for details). In our specific case four weathering cycles were carried out ($n = 4$).

2.2. NOA samples

NOA samples analysed in this pilot study are reported in Table 1. Samples were collected from serpentinites outcrops located in Elba Island (Tuscany, Italy) and province of Siena (Murlo study area).

The representativeness of the selected typology of serpentinite lithotypes for this pilot investigation was already pointed out in a work by Marzini et al. (2024) and it is here taken up schematically in Fig. 2: sample NOA1 corresponds to serpentinites deformed with a predominant brittle cataclastic mechanism (cataclastic serpentinite class); whereas NOA2 and NOA3 samples belong to "massive serpentinite" category, in which rocks are usually unaffected by weathering processes. Finally, sample NOA4 corresponds to a vein mostly formed by highly crystalline lizardite, with minor interstitial chrysotile (~8%) (Viti and Mellini, 1997).

2.3. Slake Durability Test

Slake Durability Test was carried out using the A130 apparatus (Matest®). The system incorporates a motor drive unit mounted on a baseplate which revolves four stainless steel drums manufactured from 2 mm mesh, Ø140 mm, length 100 mm. Slake Durability Test was performed following the ISRM guidelines (Ulusay and Hudson, 2007). For each serpentinite sample, pieces of about 50 g with a total weight of about 500 g were provided and tested in pure water with a temperature equal to 20 °C (Fig. 3). Slake durability rotation time was set to ten minutes with 20 rpm. After each test cycle, the specimens and the resulting powder were heated in an oven for 24 h at 105 °C to calculate the weight loss. For each cycle (SDT phase n, %), the slake durability index (SDI_n) is calculated using the following equation:

$$SDI_n = \frac{Wd_n}{Wd_0}\ 100 \quad (1)$$

Where Wd_n and Wd_0 represent dry weight of a sample after n slake cycles and the original weight of the sample, respectively (Danaei and Fereidooni, 2023).

SDT was extended from the standard two cycles to four cycles following the work of Martinez-Bofill et al. (2013) and Selen et al. (2020). According to these authors, the extension from two to four SDT cycles allows the more complete characterization of the serpentinites, revealing the progressive degradation patterns not always rising after two cycles.

Table 1
List of NOA samples selected to perform the Slake Durability Test.

ID sample	Description/Lithotype	Location
NOA1	Cataclastic serpentinite	Elba Island (Tuscany, Italy)
NOA2	Massive serpentinite	Murlo (Province of Siena, Italy)
NOA3	Massive serpentinite	Elba Island (Tuscany, Italy)
NOA4	Serpentinite with crystalline lizardite and interstitial chrysotile	Elba Island (Tuscany, Italy)

2.4. NIR-SWIR HSI instrumentation

Serpentinite samples were analysed by using a NIR-SWIR HSI instrumentation previously described (Marzini et al., 2025). The instrumentation consists of a fiber coupled optical probe/head equipped with three confocal channels for laser excitation, Vis illumination, and NIR-SWIR reflection collection. A fiber coupled supercontinuum laser with bandwidth 400–2400 nm and power of 100 mW (Samba, LEUKOS, FR) was selected as NIR-SWIR excitation source, while the

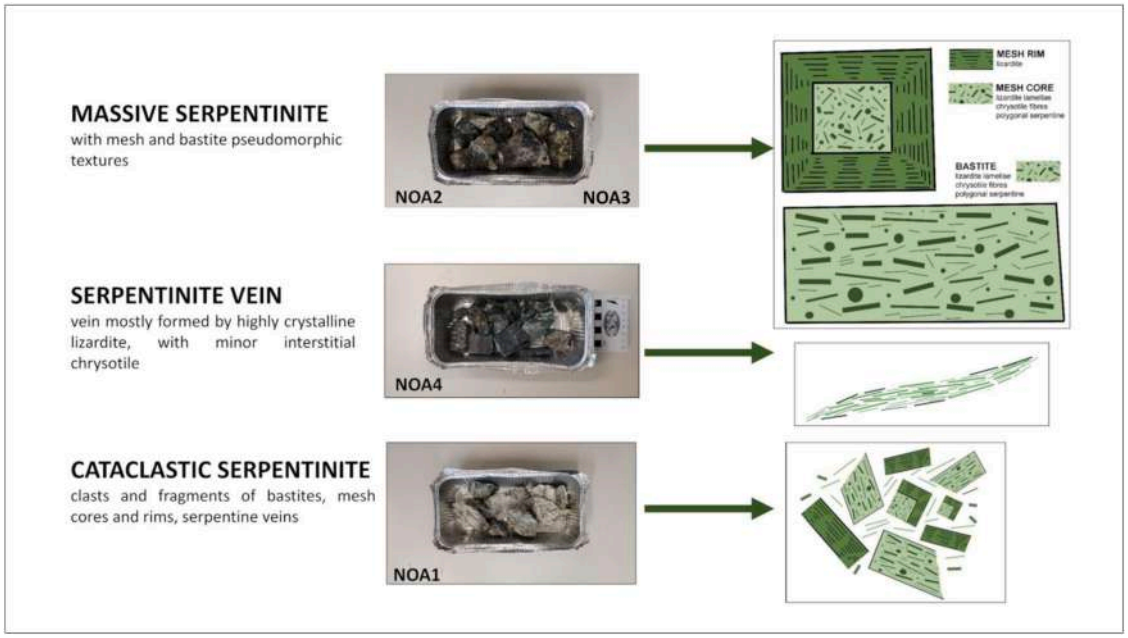

Fig. 2. Samples images and structural sketches of the three different serpentinite lithotypes selected for the pilot investigation.

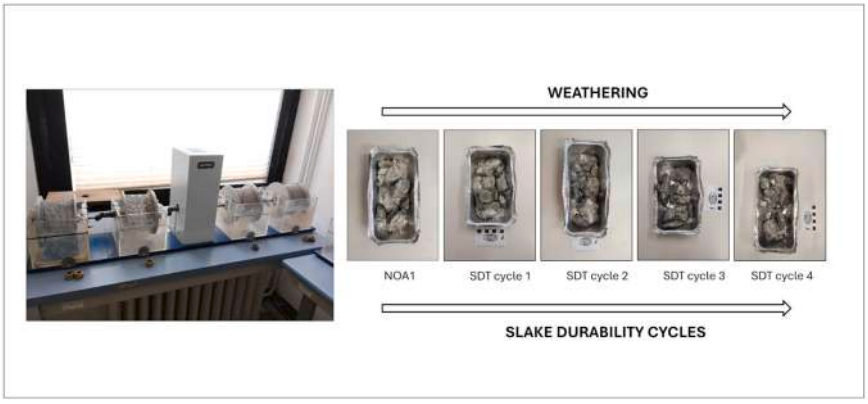

Fig. 3. Slake Durability Test apparatus (A130, Matest®) and an example of weathering evolution after four cycles of SDT (sample NOA1).

corresponding reflection signal channel was fiber coupled to the spectrometer NIRQuest+ (Ocean Optics), which was suitably customized to cover the spectral range 1350–1517 nm with a resolution of about 0.8 nm and then to detect the OH overtone bands with a rather high resolution to detect the relevant features, allowing to discriminate serpentine minerals with respect to other trioctahedral layered minerals such as talc, brucite, and chlorite (Balan et al., 2022).

The spectral power density of the laser allowed a significant reduction of the acquisition times (about 20 ms) with respect to the typical incoherent light excitation, which made it feasible the mineral scan mapping approach without any relevant risk of sample alteration. Incident power was 34 mW and single spectrum acquisition time 24 ms, which corresponds to radiant exposure producing negligible temperature rise.

In this pilot study, we use the NIR-SWIR HSI approach as a semi-quantitative mapping and screening tool for serpentine mineral group, with the limit of detection (LOD) expressed by the core diameter of the signal collection fiber, equal to 25 μm. Such approach, based also on the analysis of the standalone OH overtone band (located at about 1380 nm) is not sufficient for the discrimination among serpentine polymorphs (antigorite, chrysotile, lizardite) (Bonifazi et al., 2024; Balan et al., 2021, Laukamp et al., 2012) and, therefore, it has been coupled with the SEM and DRIFT analysis. Spectral calibration was performed using a certified 99% Spectralon® white reference. No visible damage, heating, or material removal was observed during the NIR-SWIR HSI acquisition carried out with the laser excitation. Further technical details about the instrumentation are reported in Marzini et al. (2025).

2.4.1. *Data processing*

Distribution maps of serpentine minerals within powder samples were obtained by the application of the cosine similarity method, equivalent to the spectral angle mapper (SAM) (Yuhas et al., 1992; Ramirez-Lopez et al., 2013). Such method is defined as the cosine of the plane angle between the actual spectrum vector and that of the reference (chrysotile in this study) and allows for evaluating the similarity between two spectra (sample spectra and standard spectra) represented by the respective vectors corresponding to their respective cartesian coordinates. Cosine similarity ranges between −1 (antiparallel=not similar) and 1 (parallel=maximum similarity) (Marzini et al., 2025). Chrysotile (standard sample) was provided by the Italian Workers Compensation Authority (INAIL) Department of Technological Innovations and Safety of Plants, Products and Anthropic Settlements (Rome, Italy). The performances of the selected classification method were evaluated and compared in terms of classified images and

coherence with the traditional petrographic laboratory analysis. In detail, several cosine angle thresholds were tested in order to choose the best one for this work, which ended to be equal to 0,7. Statistical analyses were performed using Origin 2018 (Origin Lab Corporation, Northampton, MA, USA, 2018).

2.5. DRIFT analysis

DRIFT analysis was carried out using an Agilent Cary 630 FTIR portable spectrometer (Agilent Technologies, Santa Clara, CA, USA) (Marzini et al., 2023). The decision to work in reflectance mode with the DRIFT method was taken due to high absorption and very low signals of the samples. DRIFT spectra were collected in the wavelength range 4000–800 cm^{-1} by 128 scans and at resolution equal to 8 cm^{-1}. Spectra were normalized against an air background recorded after each measurement. Sample preparation and data acquisition procedure still remain critical steps for the enhancement of the accuracy of the DRIFT methodology. Therefore, to verify the homogeneity of the sample, several measurements were carried out for each sample, with the final estimation of absorbance resulting from the average of the measurement values.

The Linear Calibration Curve Method (LCCM) was applied to the DRIFT spectra by plotting the peak of the absorption band as a function of asbestos concentration in different mixtures containing known quantities of standard asbestos (chrysotile):

$$h_M = B\,C_X + A \quad (2)$$

in which h_M represents the peak value of the absorption band, C_x is the analyte concentration (w/w) and A and B represent the line parameters (Accardo et al., 2014). The concentration of the asbestos within ACM sample can be obtained with the following formula:

$$C_X = \frac{(h_M - A)}{B} \quad (3)$$

Different fractions of standard mixtures of chrysotile/$CaCO_3$ (3, 6, 12, 50 and 100%, w/w) were achieved by mixing the phases in an agate mortar. Absorbance values related to the chrysotile characteristics peaks at 3690 cm^{-1} were plotted against the chrysotile concentrations for the linear fitting. Parameters obtained from the best-fit linear curve were used for the estimation of the serpentine minerals (chrysotile, lizardite and antigorite) concentration of the NOA powder samples.

2.6. Mineralogical assessment by SEM

Scanning Electron Microscope (SEM) analyses were carried out using the TESCAN VEGA 3 instrumentation, working at 20 kV of accelerating voltage, 15 μA of emission current, and 0.1 nA of beam current. The microscope is equipped with an energy-dispersive X-ray spectrometer (EDS) Bruker Quantax 200EDX for chemical microanalysis with P/B - ZAF correction method. For each sample, several areas of about 2 mm^2 were analysed. Only fibers identified as asbestos based on their composition, with a fiber length greater than 8 μm and a length-to-diameter ratio of at least 3:1 were included in the count (Boulanger et al., 2014). Regarding the fibers not entirely contained within the analysed fields, only the portions falling inside the fields were considered for the analysis (Militello et al., 2019).

3. Results

3.1. Minero-petrographic sample characterization

Sample NOA1 is a cataclastic serpentinite, in which typical pseudomorphic textures, such as meshes and bastites, have been completely disrupted and deformed. This serpentinite is further characterized by a late-stage crystallization phase, during which long fibres of chrysotile were formed pervasively in the sample. Chrysotile fibres are randomly oriented, testifying post-dynamic crystallization. Figs. 4A and C are plane-polarized light images, while 4B and 4D are the corresponding cross-polarized light images. The cataclastic texture is characterized by a fine-grained serpentine matrix cut by irregular fractures and shear zones (Figs. 4A and B). Figs. 4C and D show chrysotile elongated fibers, arranged in randomly oriented fan-shaped bundles.

NOA2 represents a typical massive pseudomorphic serpentinite formed by mesh textures and bastites. Mesh texture consists of rims (mostly formed by lizardite crystals) and cores, consisting of a complex association of nanometric lizardite, chrysotile and polygonal serpentine, occurring in random crystallographic orientations (Viti and Mellini, 1998). It is remarkable that this undeformed massive serpentinite is characterized by the abundance of sigmoidal chrysotile veins, with fibres in cross orientation. Fig. 5 reports some representative images, showing the typical petrographic characteristics of chrysotile cross veins, with anomalous high birefringence colors in crossed nicols images (Figs. 5B and D).

Sample NOA3 is a massive pseudomorphic serpentinite, associated to a crack-and-seal vein of polygonal serpentine with minor chrysotile, up to 1 cm thick. Massive serpentinite, visible in Fig. 6A and B (plane-polarized and cross-polarized light, respectively), exhibits typical mesh texture and bastite lamellae. Figs. 6C and D report the typical optical features of crack-and-seal veins formed by polygonal serpentine. Chrysotile may occur in minor sites, perpendicular to the crack-and-seal banding (Fig. 6D) and probably represents a late crystallization phase.

Sample NOA4 corresponds to a vein mostly formed by highly crystalline lizardite, with minor interstitial chrysotile (~8%). The sample has been broadly described in previous studies (MFN3 sample, e.g., in Viti and Mellini, 1997). Euhedral lizardite crystals, up to mm in size, are enveloped in minor interstitial chrysotile. Fig. 7 reports the typical texture of the lizardite vein, with rounded to elongated crystals depending on crystal orientation. In elongated crystals, (001) cleavage planes are evident.

3.2. Slake Durability Test

Fig. 8 and Table 2 show the variation of the slake durability index (SDI) after each weathering simulation (SDT) on serpentinite samples.

ISRM guidelines (1979) defines Slake Durability Index (SDI) as follows: 98 – 100 as “very high”, 95 – 98 as “high”, 85 – 95 as “medium high”, 60 –85 as “medium”, 30 – 60 as “low” and < 30 as “very low”. All the samples fall within the “very high” class meaning that these types of lithology are not inclined to realise material after SDT. In detail, referring to sample NOA1, results show the highest material loss (~ 2%) after four weathering cycles (Fig. 8), while sample NOA2 show minor weight loss (~ 1%), confirmed by the visual assessment that reveal no changes

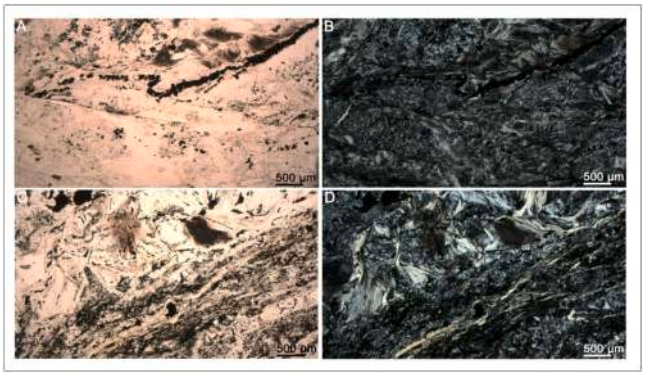

Fig. 4. Optical microscope images of NOA1: A and C are plane-plane polarized while B and cross-polarized light images. Fan-shaped chrysotile bundles are evident in C and D.

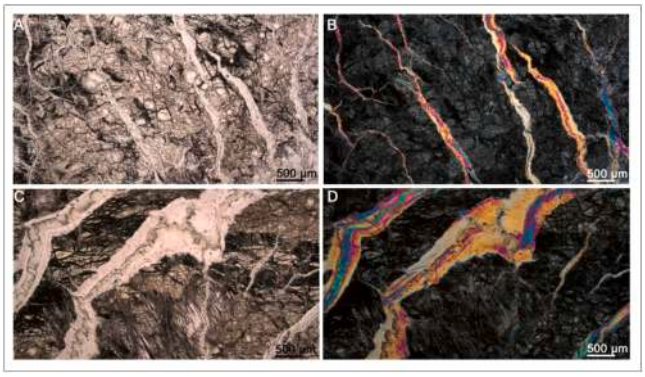

Fig. 5. Optical microscope images of NOA2. In crossed nicols polarized light (B-D) chrysotile veins display high birefringence colors up to II-order blue.

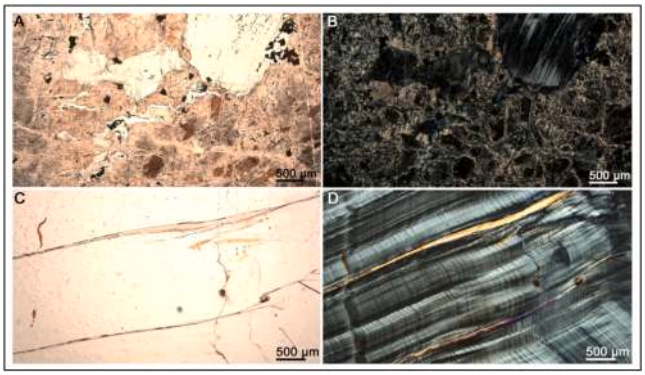

Fig. 6. Optical microscope images of NOA3: A and B correspond to the host pseudomorphic massive serpentinite, whereas C and D show crack-and-seal polygonal vein.

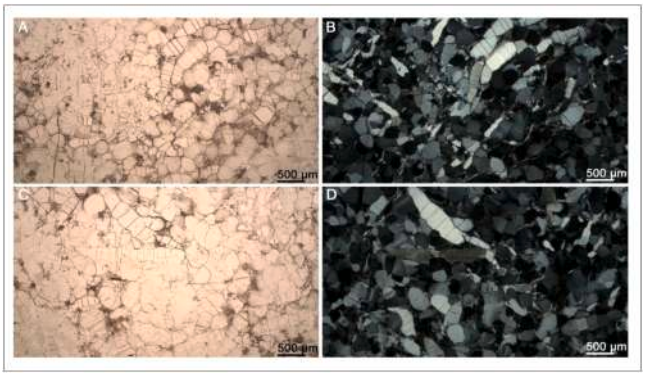

Fig. 7. Optical microscope images of sample NOA4.

for this massive sample. Analysing the SDI changes during the Slake Durability Test (Fig. 8, right side) it is possible to observe a period of stagnation (i.e., absence of changes in slake durability index, W_d ratio around 1) does not necessary correspond to a stop of the degradation phenomena (NOA1 and NOA3 samples lost material after cycle 3), confirming the decision to carry out 4 cycles.

3.3. SEM-BSE powder characterization

Fig. 9 shows representative SEM-BSE images of the material filtered after the slake durability test cycles for samples NOA1–NOA4. The images highlight the progressive mechanical evolution of the serpentinite samples after repeated wetting–drying conditions. The four samples exhibited distinct fragmentation patterns reflecting their initial textures and mineralogical composition. This distinct fragmentation pattern can be also observed analysing the numbers of fibers with fiber length > 8 µm and a length-to-diameter ratio ≥ 3:1 released by the samples (Table 3 and Fig. 10). NOA1, rich in chrysotile, released coarse fragments (>400 µm) throughout all cycles and consistently released elongated fiber bundles especially during the first two SDT cycles. In contrast, NOA2 initially produced large blocky fragments, but subsequent cycles led to progressive reduction into smaller grains; chrysotile fibers occurred only as short bundles, consistent with the nature of the samples as massive serpentinite with fibrous veins. This evidence is highlighted in Fig. 10, in which the number of hazardous fibers remains relatively constant as the number of SDT cycles gradually increases. NOA3 behaved similarly to NOA2 (with similar number of chrysotile fibres detected, see Table 4) but showed finer fragmentation earlier in the test (starting from cycle 2), reflecting its more fractured initial texture. NOA4, composed predominantly of coarse crystalline lizardite, underwent the most pronounced size reduction, with fragments becoming highly fine after the third and fourth cycles, with a corresponding increase of hazardous chrysotile fibers during the fourth cycle (Fig. 10).

3.4. NIR-SWIR HSI powder characterization

Fig. 11 shows the evolution of serpentine contents into the powder produced during the consecutive weathering simulations on the NOA samples. In contrast with the other serpentinites, NOA1 showed a decreasing trend of the serpentine contents (red colour), which range from areal ratio > 90% (after cycle 1) to < 70% (after cycle 4). This sample showed the highest release of serpentine into the powder during the first one cycle of weathering simulation, which is in agreement with its cataclastic properties (Marzini et al., 2024), (Table 1, Fig. 10). Differently, NOA2 exhibited almost constant serpentine minerals release throughout the four SDT cycles, whereas NOA3 and NOA4 showed massive release during the last two SDT cycles.

Table 4 shows the mean values of serpentine contents (SC, %) within the powder produced after the SDT cycles on rock samples. Such values were obtained by performing five random NIR-SWIR HSI maps (with a total area of 4 mm^2) for each powder sample and for each cycle for a total number of maps of 80. Referring to the powder produced during the first SDT cycle, NOA1 showed the highest serpentine content as compared to the other samples, with mean value equal to 91% (PW1).

Fig. 12 shows for each NOA sample the linear trend of the serpentine content within the powder obtained after each SDT cycle. As already mentioned, sample NOA1 shows a decreasing trend with respect to serpentine contents, with values going from > 90% (after cycle 1) to < 70% (after cycle 4) (Fig. 11, Table 4). Focusing on the other NOA samples, it can be observed that the weathering simulation produces an enrichment towards the serpentine minerals content analysed, with higher contents achieved after four SDT cycles for PW2 (~ 80%) and after three cycles for PW3 and PW4 samples (92%) (Fig. 11 and 12).

Fig. 13 shows the combined chart reporting the serpentine content (obtained with the NIR-SWIR HSI mapping) and the number of hazardous fibres (obtained through the SEM analysis) variation as the cycles of SDT increases. With this type of data visualization, the distinct fragmentation patterns exhibited by the four serpentinite samples is pronounced. Despite the limited number of serpentinite samples analysed in this pilot investigation, the fibrous habit of the cataclastic serpentinite (NOA1 sample) influenced the release of hazardous chrysotile fibers from the beginning of the weathering simulation. On the other hand, the compact and interpenetrated nanostructure of chrysotile fibers and lizardite lamellae in meshes and bastites within the massive serpentinites (NOA2 and NOA3 samples) hampers the release of large amounts of inhalable asbestos fibers during the stages of weathering.

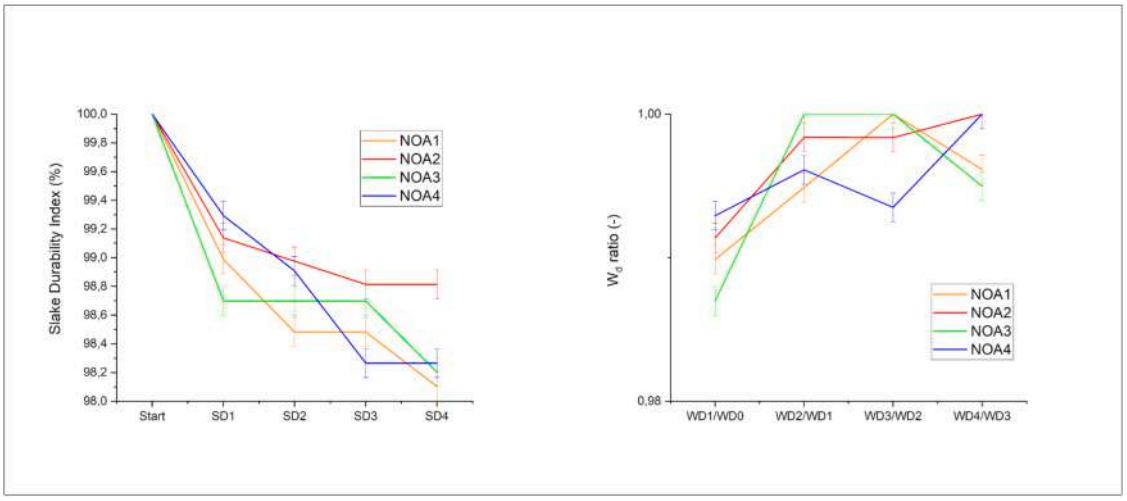

Fig. 8. Slaking evolution (in terms of Slake Durability Index-SDI, %) of the serpentinite samples during the Slake Durability Tests (left side); Wd ratio (-) evolution during the Slake Durability Test (right side); error bars determined by the precision of the analytical balance used in the SDT measurements.

Table 2
Slake Durability Index (SDI) results.

ID sample	SDI_1	SDI_2	SDI_3	SDI_4	ISRM classification
NOA1	99,0	98,5	98,5	98,1	Very High
NOA2	99,1	99,0	98,8	98,8	Very High
NOA3	98,7	98,7	98,7	98,2	Very High
NOA4	99,3	98,9	98,9	98,3	Very High

3.5. DRIFT

To validate the quantitative results obtained with the NIR-SWIR HSI technique, a LCC was applied to the DRIFT spectra of different mixtures containing known quantities of standard chrysotile and then compared with DRIFT spectra of NOA powder samples. Fig. 14 shows an example of the DRIFT spectrum of NOA4. All the samples showed the band at 3690 cm^{-1} along with the less intense band at 3645 cm^{-1}. These can be ascribed to the stretching of the external OH located at the top of the trioctahedral layer pointing to the O atoms of basal plane of the next T–O silicate layer (Fritsch et al., 2021). The other bands can be assigned to the C—O (3020–2879, 2522, 1800, 1636 cm^{-1}) of the carbonate matrix, Si-O-Si (1098 cm^{-1}) and S-O (1200 cm^{-1}) functional groups within the matrix containing the serpentine minerals.

Fig. 15A shows the LCCM (Eq. (2)) curve (with the related slope,

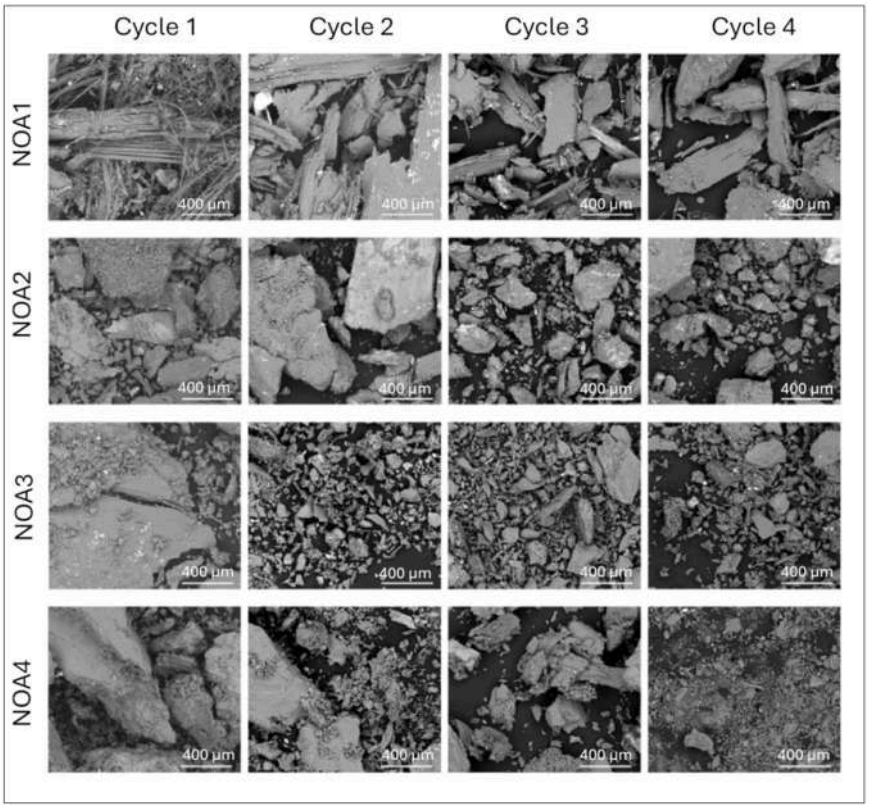

Fig. 9. SEM-BSE examples images of filtered material from samples NOA1–NOA4 after consecutive slake durability test cycles.

Table 3
Number of fibres (nf) and related standard error of the mean-SEM within the rock powder (PW) for each Slake Durability Test cycle ($_n$).

ID sample	ID Powder	nf_1	nf_1 SEM	nf_2	nf_2 SEM	Nf_3	nf_3 SEM	nf_4	nf_4 SEM
NOA1	PW1	76	9	31	3	12	4	20	2
NOA2	PW2	108	14	28	3	20	2	19	3
NOA3	PW3	15	2	19	1	22	6	21	1
NOA4	PW4	14	4	19	1	19	5	91	1

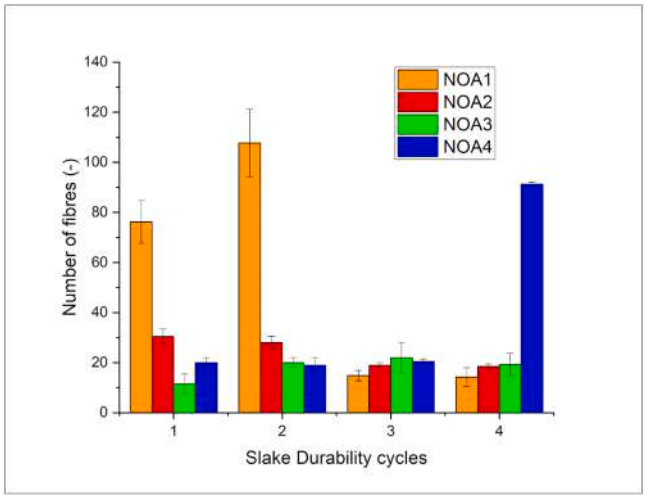

Fig. 10. Number of asbestos fibres counted (fiber length > 8 μm and a length-to-diameter ratio ≥ 3:1) after the SDT cycles (error bars determined by the Standard Error of the Mean).

intercept and errors) of the DRIFT OH fundamental vibration band of chrysotile (3690 cm^{-1}) as derived by measuring standard mixtures of pure chrysotile and $CaCO_3$. The basic assumption of the linear relationship between the chrysotile concentration and the integrated intensity of such mentioned absorption band has been verified (Pearson' R equal to 0.99; adjusted R^2 equal to 0.99) (Fig. 15A). By using the calibration curve parameters and Eq. (3), the serpentine concentration values related to NOA powder samples (Fig. 15B) was obtained. Results are in agreement with the SC_{mean} serpentine contents obtained from the NIR-SWIR HSI analysis (Table 4), thus demonstrating the capability of NIR-SWIR HSI technique in quantifying serpentine's minerals. Data showed high values of serpentine contents, with an average serpentine concentration equal to 77.5%, in good agreement with the mean SC values obtained by NIR-SWIR HSI (Table 4).

4. Discussion

Results achieved in this pilot investigation prove that whisk broom portable NIR-SWIR HSI is very efficient in mapping serpentine minerals in rock and powder samples, which can safely be achieved in situ without any preliminary sample preparation, thus preventing risks of inhalation of asbestos fibers. Thanks to the narrow collection fiber, (⌀50 μm core) and very short scan step (10 μm), lateral spatial resolution of about 25 μm was achieved, which allowed collecting serpentine distribution in powders produced during SDT, such as those displayed in Fig. 11. These results represent a starting point for in situ qualitative and semi-quantitative evaluation of the serpentine contents in serpentinites and the accurate determination release index in laboratory tests.

Here, the different content of serpentine in the released powders produced during SDT cycles can be explained in terms of different nanostructure of chrysotile fibers and lizardite lamellae in meshes and bastites as shown in Fig. 2 (Marzini et al., 2024) highlighting that in NOA the detection of fibers is a parameter as important as their capability to be released. In this respect, the use of a NIR-SWIR hyperspectral portable tool to carry out fast mineral maps of the rock in the form of powder or small flat slice, represents an effective innovative approach. NIR-SWIR HSI approach provides detailed mineral maps with minimal temporal efforts. As an example, the overall scanning time and map visualization for a sample surface of about 1 cm^2, with a spatial resolution of 10 μm and an integration time of about 24 ms, corresponding to 1 million spectra, is about 1 hour (Marzini et al., 2025). It is highlighted that such analysis does not require a manipulation/alteration of the samples, with the detection limit of the analysis equal to the core diameter of the signal collection fiber used (25 μm in this case), assuring a very high in situ portability.

Despite the strong durability of the serpentinite samples selected in this work, (all classified as "very high"), differences among the samples in terms of serpentine minerals contents were detected due to their different lithology (Fig. 2, Fig. 10 and Fig. 11). NOA1 sample exhibited the highest values of serpentine distribution after one SDT cycle and a decreasing trend during the following weathering simulations. This result could strongly be affected by the fibrous splintery veins of the samples. On the other hand, the compact and interpenetrated nanostructure of chrysotile fiber and lizardite lamellae in meshes and bastites within the massive serpentinites (NOA2, NOA3) hampers the release of inhalable asbestos fibers during the stages of weathering (Fig. 11). In this respect, the slight difference between DRIFT and NIR-SWIR HSI analyses was due to the known limits of DRIFT methodology to the analysis of heterogeneous samples (such as our powders and soils) (Manley, 2014; Pudełko et al., 2020). Considering the NIR-SWIR HSI and SDT results it can be observed an apparent paradox: all the serpentinites analysed fall within the class "very high" of ISRM classification (Table 2), exhibiting very high Slake Durability Index values. Despite the high resistance to mechanical wetting and drying cycles of the samples (SDI > 98%), hyperspectral imaging and SEM analysis carried out on the powder produced after the weathering simulation highlight the presence of hazardous asbestos fibers (Fig. 13). This apparent contradiction between the small amount of material lost and the significant number of asbestos fibers detected can be explained in terms of spatial distribution of the fibrous portion of the serpentinites. Indeed, the Slake Durability Index is a gravimetric parameter that, if considered standalone, does not

Table 4
Serpentine areal ratios (%) and standard error of the mean-SEM related to rock powder (PW) for each Slake Durability Test cycle.

ID sample	ID Powder	SC_1 (%)	SC_1 SEM (%)	SC_2 (%)	SC_2 SEM (%)	SC_3 (%)	SC_3 SEM (%)	SC_4 (%)	SC_4 SEM (%)
NOA1	PW1	91	4	79	2	73	3	68	4
NOA2	PW2	59	1	73	3	68	3	80	6
NOA3	PW3	37	4	43	5	92	3	98	1
NOA4	PW4	34	5	66	1	92	3	98	2

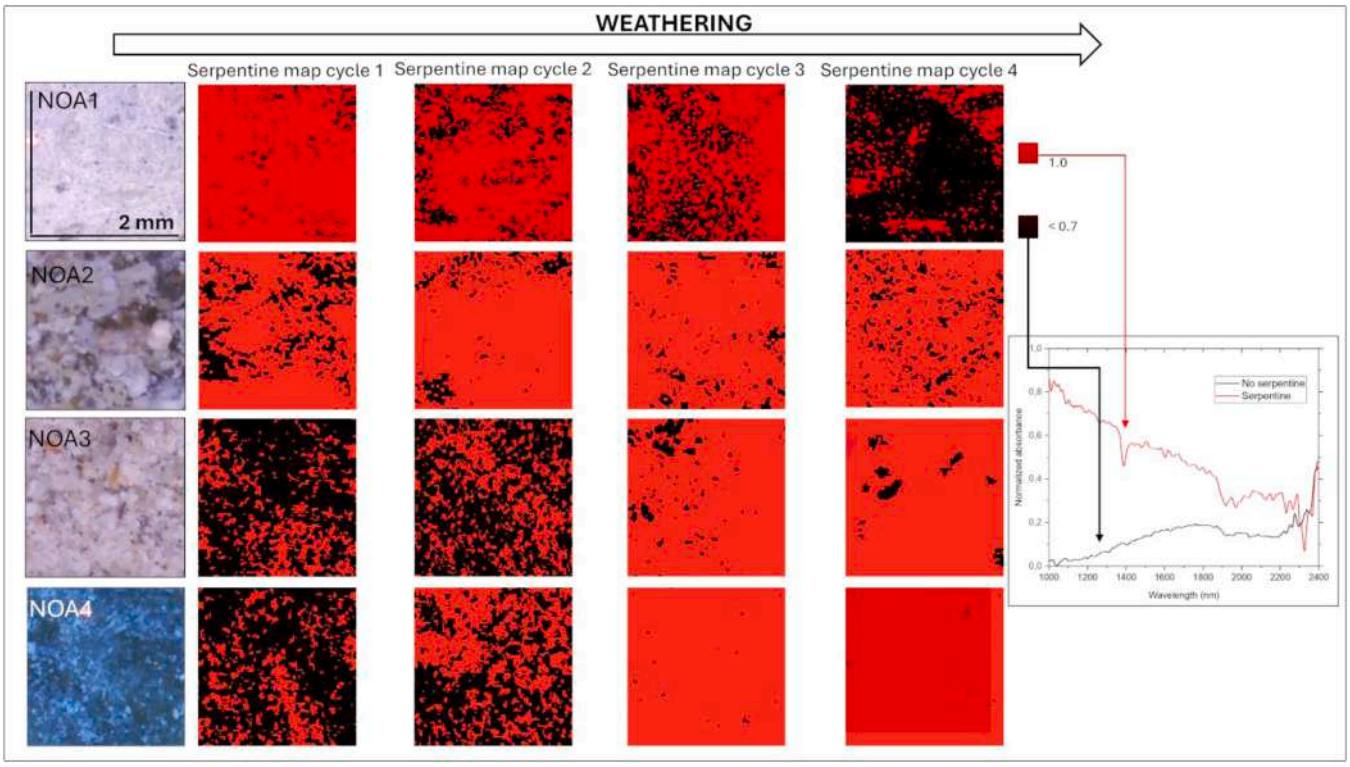

Fig. 11. Areal mapping of the serpentine distribution into the powder produced during the weathering simulation on the NOA samples, as derived using the cosine spectral metrics over the OH overtone wavelength range around 1380 nm (Balan et al., 2021; Laukamp et al., 2012; Marzini et al., 2025).

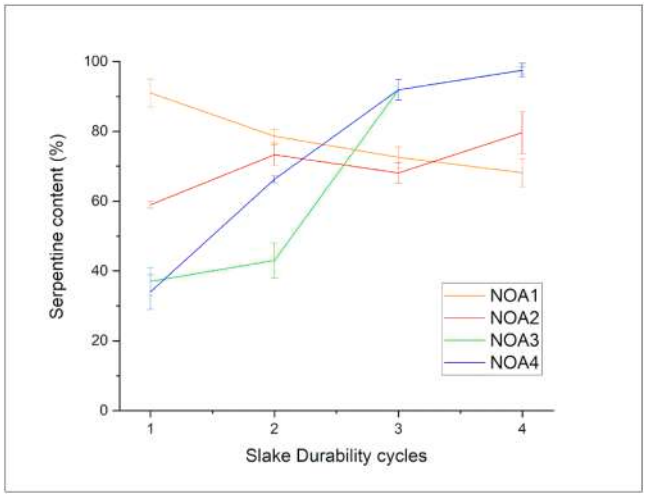

Fig. 12. Serpentine content variation as the number of SDT cycles increases.

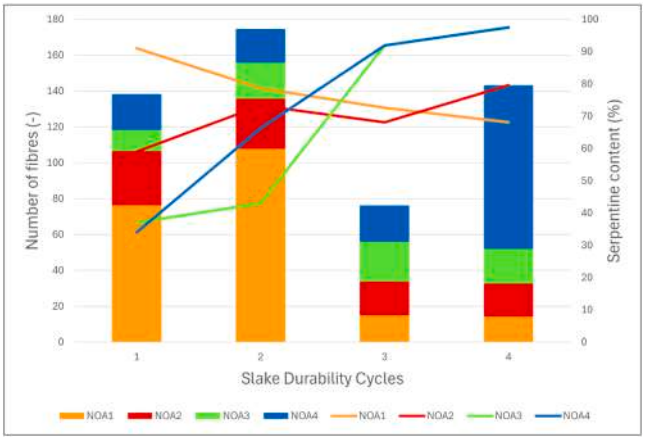

Fig. 13. Combined chart reporting the serpentine content variation (lines) and the number of chrysotile fibres variation (boxes) as the number of SDT cycles increases (lines).

provide information about the mineralogical composition of the released material and the selectivity of the weathering process towards the lithotype analysed (Selen et al., 2020). The overall structure together with the initial degree of micro-fracturing of the sample plays a relevant role towards the water infiltration into the material (Dick and Shakoor, 1992). Asbestos fibers in serpentinites are typically confined to veins, fractures, and schistosity planes, which represent zones of preferential losses as compared to the massive matrix (Gaggero et al., 2013; Marzini et al., 2024; Santo et al., 2025). During the Slake Durability Test, the combined action of water, mechanical abrasion and thermal expansion determine the selective release of fibres, even in the absence of significant degradation of the total mass (Table 2). This characteristic mechanism of serpentinites emphasizes the importance of combine SDT with compositional analysis of the released powder (such as those carried out in this investigation pilot) for a reliable assessment of the potential release of asbestos fibres (Singh et al., 2025).

Unfortunately, the NIR-SWIR HSI approach, based on the analysis of the standalone OH overtone band (located at about 1380 nm) is not sufficient for the discrimination among serpentine polymorphs (antigorite, chrysotile, lizardite) (Bonifazi et al., 2024; Balan et al., 2021, Laukamp et al., 2012). Indeed, the crystallographic differences among the polymorphs are represented by deformation and disposition of the two-layer structure T-O (Demichelis et al., 2016; Fritsch et al., 2021) not allowing such discrimination (Balan et al., 2002). Therefore, our results, expressed in terms of release index of serpentine mineral group, can be considered a cautionary approach since not all the serpentine minerals

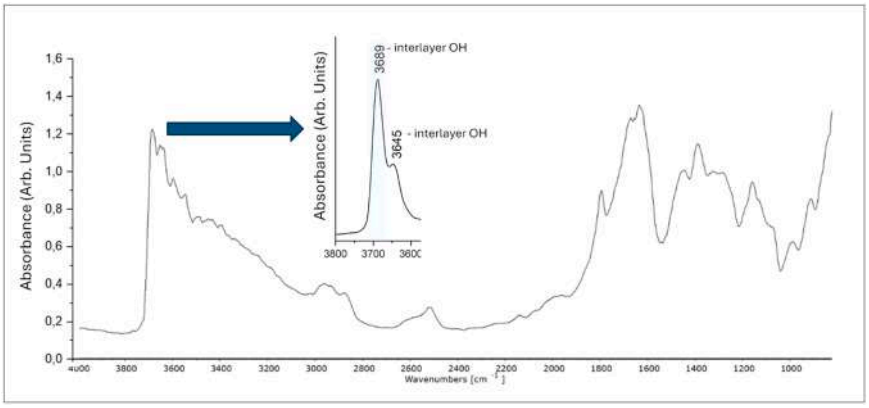

Fig. 14. DRIFT spectra of the NOA4 powder sample (bands related to the stretching of the interlayer OH are displayed in the enlarged box, with the peak at around 3690 cm^{-1} (light blue colour) used as analytical band for the DRIFT analysis).

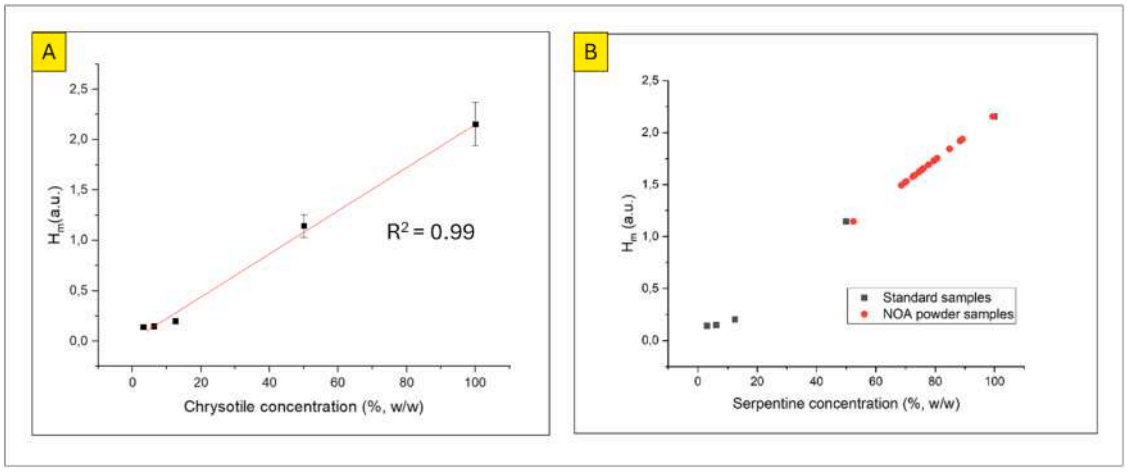

Fig. 15. Linear Calibration Curve Method results (A: chrysotile/CaCO3 mixtures, black squares; B: NOA powder samples at different SDT analysed, red points).

detected in the maps correspond to chrysotile phase, as it was also pointed out by the minero-petrographic characterization. However, it must be taken into account that, during the last years, the toxicological profile of antigorite has been pointed out in several studies (see for example Gazzano et al., 2023; Petriglieri et al., 2023, 2025), which suggest to identify and quantify the whole serpentine in release studies due to the growing awareness about the pathogenicity of fibrous antigorite, with examples from the Calabrian (Italy), and New Caledonia (France) serpentinites (Gazzano et al., 2023; Petriglieri et al., 2025) and the lack of sufficient in vivo and in vitro studies about fibrous lizardite (Militello et al., 2021).

In this work, weathering simulations were carried out by alternating wetting and dry cycles, but other mechanisms can affect the rock durability, especially in severe environmental conditions (Franklin and Chandra, 1972). The amount, the distribution, and the potential release of chrysotile fibers, for example, are mostly driven by deformation type and outcrop extent. The present results are congruent with the qualitative hazard scale which indicates lower risk for the massive with respect to cataclastic serpentinite. However, they also show that even massive lithologies exhibit increased serpentine (chrysotile) release after some cycles. In the literature, an attempt towards the evaluation of the asbestos hazard related to a generic serpentinite outcrop was carried out by Gaggero et al. (2013). This proposed an engineering geological protocol considering the mineralogical, petrological, and geotechnical features of serpentinites, leading to a quantitative determination of the asbestos contents in bulk samples. At the same time, we strongly believe that weathering process of rocks must be taken into account for a more reliable and complete hazard assessment of NOA. In this respect, the Slake Durability Tests plays a crucial role for describing the tendency of the rock to release fibers in the environment. As a matter of fact, several studies concerning ACM and NOA characterizations mention the weathering action without providing detailed information about the chemical and physical effects it produced (Cilia et al., 2015; Gaggero et al., 2013; Malinconico et al., 2022). This work represents a step ahead to fill this gap. However, focusing on the simulation of weathering carried out in this pilot investigation, it must be noted that the physicochemical processes that affects the fiber release from NOA are different from those simulated by SDT. Indeed, the mechanical abrasion and crushing that occur into the steel drums of the A130 apparatus (Matest®) do not replicates the same high-energy impacts and grinding related to excavation or rock crushing for industrial productions. Moreover, atmospheric agents (acid rain), bio-weathering actions (lichens, fungi), and saline solutions in coastal environments can alter mineral surfaces with the consequent reduction of cohesion (Favero-Longo et al., 2009, 2013; Taylor et al., 2024). SDT do not consider these agents. Being aware of these limitations, SDT can be ascribed as a controlled and replicable (due to the standardization and comparability across different lithologies and study sites) laboratory stress regime for material durability assessment. Fiber release results obtained in this pilot study suggest that NOA-bearing serpentinites can release hazardous fibres under minimal mechanical disturbance (low energy, absence of thermal extremes), with implications for their manipulation/alteration in anthropic environments. In this context, we propose the SDT, when coupled with compositional analysis, as a

screening tool for the assessment of the hazard potential related to asbestos fibres, useful towards the selection of samples for the subsequent more detailed (and expensive) traditional laboratory analysis.

5. Conclusions

In this pilot investigation, simulated weathering of a small set of serpentinite rock samples has been carried out through the Slake Durability Test (SDT) for evaluating their respective release of serpentine minerals during wet and dry cycles. Serpentinite rock powders resulting from these weathering processes were then analysed by means of an innovative portable NIR-SWIR hyperspectral imaging instrument for quantifying the contents of serpentine minerals. The results achieved were successfully validated using SEM and FTIR analyses. Such an innovative combined approach based on SDT, NIR-SWIR HSI and SEM techniques allowed for collecting information on durability properties of serpentinite rocks and rapidly evaluating the respective serpentine release index during the weathering simulation. Despite the set of samples selected in this study were homogeneous in terms of durability (class "very high" according to the ISRM classification system), different serpentine mineral release trends were measured during consecutive cycles, which were validated as mentioned above. This demonstrated the reliability of the novel HSI tool and its effectiveness in quantifying the risk associated with the use of the present NOA rocks in urban environment when used in combination with SDT. Further insights will be dedicated to the refinement of the analytical procedure that can be extended for the study of other naturally occurring asbestos samples (e.g., metabasites, ophicalcites) and other serpentinites lithotypes with different fabrics and metamorphic grades.

Funding information

This work was co-funded by Italian Workers Compensation Authority (INAIL) and Consiglio Nazionale delle Ricerche (CNR).

CRediT authorship contribution statement

Lorenzo Marzini: Writing – original draft, Visualization, Validation, Methodology, Investigation, Formal analysis, Conceptualization. **Daniele Ciofini:** Writing – review & editing, Writing – original draft, Methodology. **Juri Agresti:** Writing – review & editing. **Andrea Azelio Mencaglia:** Writing – review & editing, Visualization, Software. **Leonardo Disperati:** Writing – review & editing. **Narcisa Mihaela Marian:** Visualization, Investigation, Formal analysis. **Nadia Valletti:** Visualization, Investigation, Formal analysis. **Cecilia Viti:** Writing – review & editing. **Sergio Bellagamba:** Funding acquisition. **Sergio Malinconico:** Funding acquisition. **Federica Paglietti:** Funding acquisition. **Salvatore Siano:** Writing – review & editing, Resources, Funding acquisition. **Iacopo Osticioli:** Writing – original draft, Supervision, Methodology, Conceptualization.

Declaration of competing interest

The authors declare that they have no known competing financial interests or personal relationships that could have appeared to influence the work reported in this paper.

Acknowledgements

The present work was carried out within the activities of the project SIC-QUAM "*Development of chemical imaging instrumentation for the identification and* in situ *quantitative evaluation of asbestos fiber content in ACM*" co-funded by INAIL (BRIC 2022, ID 70).

Data availability

All data generated or analysed for this study are included in this article, and the related datasets are available from the corresponding author upon reasonable request.

References

Accardo, G., Cioffi, R., Colangelo, F., D'Angelo, R., De Stefano, L., Paglietti, F., 2014. Diffuse reflectance infrared fourier transform spectroscopy for the determination of asbestos species in bulk building materials. Materials 7, 457–470.

Balan, E., Saitta, A.M., Mauri, F., Lemaire, C., Guyot, F., 2002. First-principles calculation of the infrared spectrum of lizardite. Am. Miner. 87, 1286–1290. https://doi.org/10.2138/am-2002-1003.

Balan, E., Fritsch, E., Radtke, G., Paulatto, L., Juillot, F., Baron, F., Petit, S., 2021. First-principles modeling of the infrared spectrum of Fe- and Al-bearing lizardite. Eur. J. Miner. 33, 647–657. https://doi.org/10.5194/ejm-33-647-2021.

Balan, E., Paulatto, L., Deng, Q., Béneut, K., Guillaumet, M., Baptiste, B., 2022. Molecular overtones and two-phonon combination bands in the near-infrared spectra of talc, brucite and lizardite. Eur. J. Mineral. 34, 627–643. https://doi.org/10.5194/ejm-34-627-2022.

Bauer, S.J., Friedman, M., Handin, J., 1981. Effects of Water-Saturation on Strength and Ductility of Three Igneous Rocks at Effective Pressures to 50MPa and Temperatures to Partialmelting. Texas A and M Univ., College StationUSA https://doi.org/10.2172/6381419. Technical ReportCenter for Tectonophysics.

Bellagamba, S., Paglietti, F., Malinconico, S., Bonifazi, G., Serranti, S., Aurigemma, A., 2024. Remediation Activities in Italian Superfund Sites: the case study of Naples - Bagnoli. In: Proceedings of the 10th World Congress on New Technologies (NewTech'24). Barcelona, Spain. Paper No. ICEPR 145.

Bloise, A., Miriello, D., 2018. Multi-analytical approach for identifying asbestos minerals in situ. Geosciences 8, 133.

Bloise, A., Miriello, D., 2022. Distinguishing asbestos cement from fiber-reinforced cement through portable μ-Raman spectroscopy and portable X-ray fluorescence. Env. Monit. Assess. 194 (10), 679. https://doi.org/10.1007/s10661-022-10343-x.

Bonatti, E., Michael, P.J., 1989. Mantle peridotites from continental rifts to ocean basins to subduction zones. Earth Planet. Sci. Lett. 91 (3–4), 297–311. https://doi.org/10.1016/0012-821X(89)90005-8. ISSN 0012-821X.

Bonifazi, G., Capobianco, G., Serranti, S., 2018. Asbestos containing materials detection and classification by the use of hyperspectral imaging. J. Hazard. Mater 344, 981–993. https://doi.org/10.1016/j.jhazmat.2017.11.056.

Bonifazi, G., Capobianco, G., Serranti, S., 2019. Hyperspectral imaging and hierarchical PLS-DA applied to asbestos recognition in construction and demolition waste. Appl. Sci. 9 (21), 4587. https://doi.org/10.3390/app9214587.

Bonifazi, G., Capobianco, G., Serranti, S., Malinconico, S., Paglietti, F., 2022. Asbestos detection in construction and demolition waste adopting different classification approaches based on short wave infrared hyperspectral imaging. Detritus 20, 90–99. https://doi.org/10.31025/2611-4135/2022.15211.

Bonifazi, G., Capobianco, G., Serranti, S., Trotta, O., Bellagamba, S., Malinconico, S., Paglietti, F., 2024. Asbestos detection in construction and demolition waste by different classification methods applied to short-wave infrared hyperspectral images. Spectrochim. Acta Mol. Biomol. Spectrosc. 307, 123672. https://doi.org/10.1016/j.saa.2023.123672.

Boulanger, G., Andujar, P., Pairon, J.C., Billon-Galland, M.A., Dion, C., Dumortier, P., Brochard, P., Sobaszek, A., Bartsch, P., Paris, C., Jaurand, M.C., 2014. Quantification of short and long asbestos fibers to assess asbestos exposure: a review of fiber size toxicity. Env. Health 13, 59. https://doi.org/10.1186/1476-069X-13-59.

Carmignano, O.R.D.R., Brandao, P.R.G., 2023. Employment of serpentinite rock in architecture. Mater. Sci. Eng. 7 (2), 79–81. https://doi.org/10.15406/mseij.2023.07.00208.

Cilia, C., Panigada, C., Rossini, M., Candiani, G., Pepe, M., Colombo, R., 2015. Mapping of asbestos cement roofs and their weathering status using hyperspectral aerial images. ISPRS Int. J. Geo-Inf. 4, 928–941. https://doi.org/10.3390/ijgi4020928.

Cossio, R., Albonico, C., Zanella, A., Fraterrigo-Garofalo, S., Avatenoe, C., Compagnoni, R., Turci, F., 2018. Innovative unattended SEM-EDS analysis for asbestos fiber quantification. Talanta 190, 158–166.

Curado, A., Nunes, L.J.R., Carvalho, A., Abrantes, J., Lima, E., Tomé, M., 2024. The use of asbestos and its consequences: an assessment of environmental impacts and public health risks. Fibers 12, 102. https://doi.org/10.3390/fib12120102.

Danaei, S., Fereidooni, D., 2023. On the importance of specimen's geometric shape effects on the slake-durability index of limestones and grain size distribution of the sediment particles obtained during the test. Constr. Build. Mater. 394, 132205. https://doi.org/10.1016/j.conbuildmat.2023.132205. ISSN 0950-0618.

Demichelis, R., De La Pierre, M., Mookherjee, M., Zicovich-Wilson, C.M., Orlando, R., 2016. Serpentine polymorphism: a quantitative insight from first-principles calculations. CrstEngComm 18, 4412–4419. https://doi.org/10.1039/c6ce00190d.

Dick, J.C., Shakoor, A., 1992. Lithological controls of mudrock durability. Q. J. Eng. Geol. Hydrogeol. 25 (1), 31–46.

Favero-Longo, S.E., Turci, F., Tomatis, M., Compagnoni, R., Piervittori, R., Fubini, B., 2009. The effect of weathering on ecopersistence, reactivity and potential toxicity of naturally occurring asbestos and asbestiform minerals. J. Toxicol. Environ. Health A 72, 305–314.

Favero-Longo, S.E., Turci, F., Fubini, B., Castelli, D., Piervittori, R., 2013. Lichen deterioration of asbestos and asbestiform minerals of serpentinite rocks in Western Alps. Int. Biodeterior. Biodegrad. 84, 342–350. https://doi.org/10.1016/j.ibiod.2012.07.018.

Franklin, J.A., Chandra, R., 1972. The slake-durability test. Int. J. Rock Mech. Min. Sci. Geomech. Abstr. 9 (3), 325–328.

Fritsch, E., Balan, E., Petit, S., Juillot, F., 2021. Structural, textural, and chemical controls on the OH stretching vibrations in serpentine-group minerals. Eur. J. Miner. 33, 447–462. https://doi.org/10.5194/ejm-33-447-2021.

Gaggero, L., Crispini, L., Isola, E., Marescotti, P., 2013. Asbestos in natural and anthropic ophiolitic environments: a case study of geohazards related to the northern Apennine ophiolites (eastern Liguria, Italy). Ofioliti 38, 29–40.

Gazzano, E., Petriglieri, J.R., Aldieri, E., Fubini, B., Laporte-Magoni, C., Pavan, C., Tomatis, M., Turci, F., 2023. Cytotoxicity of fibrous antigorite from New Caledonia. Env. Res. 230, 115046. https://doi.org/10.1016/j.envres.2022.115046.

Haldar, S.K., 2020. In: Introduction to Mineralogy and Petrology, Second Edition, p. 436. https://doi.org/10.1016/C2019-0-00625-5.

Harper, M., 2008. 10th anniversary critical review: naturally occurring asbestos. J. Env. Monit. 10, 1394–1408. https://doi.org/10.1039/B810541N.

Hu, K., Feng, Q.S., Wang, X., 2017. Experimental research on mechanical property of phyllite tunnel surrounding rock under different moisture state. Geotech. Geol. Eng. 35 (1), 303–311.

ISRM, 1979. Suggested methods for determining water content, porosity, density, absorption and related properties and swelling and slake durability index properties: part 1: suggested methods for determining water content, porosity, density, absorption and related properties. Int. J. Rock Mech. Min. Sci. Geomech. Abstr. 16 (2), 143–151.

Laukamp, C., Termin, K.A., Pejcic, B., Haest, M., Cudahy, T., 2012. Vibrational spectroscopy of calcic amphiboles-applications for exploration and mining. Eur. J. Miner. 24 (5), 863–878. https://doi.org/10.1127/0935-1221/2012/0024-2218.

Malinconico, S., Paglietti, F., Serranti, S., Bonifazi, G., Lonigro, I., 2022. Asbestos in soil and water: a review of analytical techniques and methods. J. Hazard. Mater. 436, 129083. https://doi.org/10.1016/j.jhazmat.2022.129083. ISSN 0304-3894.

Manley, M., 2014. Near-infrared spectroscopy and hyperspectral imaging: non-destructive analysis of biological materials. Chem. Soc. Rev. 43 (24), 8200–821421. Open Access.

Martinez-Bofill, J., Corominas Dulcet, J., Soler Gil, A., Polvoreda, R., Navarro, J.A., 2013. Propuesta de mejora de la sensibilidad del ensayo Slake Durability Test para la caracterización de taludes excavados en rocas arcillosas. A: simposio nacional sobre taludes y laderas inestables. VIII Simposio Nacional Sobre Taludes y Laderas Inestables. Palma de Mallorca, pp. 207–218.

Marzini, L., Ciofini, D., Agresti, J., Ciaccheri, L., D'Addario, E., Disperati, L., Siano, S., Osticioli, I., 2023. Exploring the potential of portable spectroscopic techniques for the biochemical characterization of roots in shallow landslides. Forests 14, 825. https://doi.org/10.3390/f14040825.

Marzini, L., Iannini, M., Giorgetti, G., Bonciani, F., Conti, P., Salvini, R., Viti, C., 2024. Asbestos hazard in serpentinite rocks: influence of mineralogical and structural characteristics on Fiber potential release. Geosciences 14, 210. https://doi.org/10.3390/geosciences14080210.

Marzini, L., Osticioli, I., Ciofini, D., Agresti, J., Bellagamba, S., Paglietti, F., Mencaglia, A. A., Siano, S., 2025. Identification, mapping, and quantification of asbestos minerals in ACM and NOA using NIR-SWIR hyperspectral scan imaging: preliminary study. Spectrachim. Acta A. https://doi.org/10.1016/j.saa.2025.125893.

Mevel, C., 2003. Serpentinization of abyssal peridotites at mid-ocean ridges Serpentinisation des péridotites abysales aux dorsales océaniques. C. R. Geosci. 335, 825–852.

Militello, G.M., Sanguineti, E., Yus González, A., Mantovani, F., Gaggero, L., 2019. The concentration of asbestos fibers in bulk samples and its variation with grain size. Minerals 9, 539. https://doi.org/10.3390/min9090539.

Militello, G.M., Gaggero, L., La Maestra, S., 2021. Asbestiform amphiboles and cleavage fragments analogues: overview of critical dimensions, aspect ratios, exposure and health effects. Minerals 11 (5), 525. https://doi.org/10.3390/min11050525.

O'Hanley, D.S., 1996. Serpentinites: Records of Tectonic and Petrological History, Oxford Monographs on Geology and Geophysics. Oxford University Press. ISSN 0952-7028.

Petriglieri, J.R., Laporte-Magoni, C., Salvioli-Mariani, E., Tomatis, M., Gazzano, E., Turci, F., Cavallo, A., Fubini, B., 2020. Identification and preliminary toxicological assessment of a non-regulated mineral fiber: fibrous antigorite from New Caledonia. Env. Eng. Geosci. XXVI, 89–97.

Petriglieri, J.R., Barale, L., Viti, C., Ballirano, P., Belluso, E., Bruno, M.R., Campopiano, A., Cannizzaro, A., Fantauzzi, M., Gianchiglia, F., Montereali, M.R., Nardi, E., Olori, A., Piana, F., Tomatis, M., Rossi, A., Skogby, H., Pacella, A., Turci, F., 2023. From field analysis to nanostructural investigation: a multidisciplinary approach to describe natural occurrence of asbestos in view of hazard assessment. J. Hazard. Mater. 457, 131754. https://doi.org/10.1016/j.jhazmat.2023.131754.

Petriglieri, J.R., Capitani, G., Ballirano, P., Barale, L., Piana, F., Tomatis, M., Di Carlo, M. C., Gianchiglia, F., Campopiano, A., Olori, A., Bruno, M.R., Montereali, M.R., Nardi, E., Fantauzzi, M., Rossi, A., Skogby, H., Belluso, E., Turci, F., Pacella, A., 2025. Naturally occurring asbestos in southern Italy: geological and mineralogical investigation of fibrous antigorite from Calabrian serpentinites in view of its hazard assessment. Sci. Total Environ. 970, 178970. https://doi.org/10.1016/j.scitotenv.2025.178970. ISSN 0048-9697.

Pudełko, A., Chodak, M., Roemer, J., Uhl, T., 2020. Application of FT-NIR spectroscopy and NIR hyperspectral imaging to predict nitrogen and organic carbon contents in mine soils. Measurement 164, 108117. https://doi.org/10.1016/j.measurement.2020.108117. ISSN 0263-2241.

Punturo, R., Ricchiuti, C., Bloise, A., 2019. Assessment of serpentine group minerals in soils: a case study from the village of San Severino Lucano (Basilicata, Southern Italy). Fibers 7, 18.

Ramirez-Lopez, L., Behrens, T., Schmidt, K., Viscarra Rossel, R.A., Demattê, J.A.M., Scholten, T., 2013. Distance and similarity-search metrics for use with soil vis–NIR spectra. Geoderma 199, 43–53. https://doi.org/10.1016/j.geoderma.2012.08.035. ISSN 0016-7061.

Rivero Crespo, M.A., Pereira Gómez, D., Villa García, M.V., Gallardo Amores, J.M., Sánchez Escribano, V., 2019. Characterization of serpentines from different regions by transmission electron microscopy, X-ray diffraction, BET specific surface area and vibrational and electronic spectroscopy. Fibers 7, 47.

Saba, M., Castrillón-Ortíz, C., Torres-Ortega, R., Coronado-Hernández, O.E., Bustillo-LeCompte, C., 2026. Affordable risk mapping and detection of asbestos-cement roofs via remote sensing: towards accessible urban digital twins in low- to middle-income countries. J. Env. Manage. 401. https://doi.org/10.1016/j.jenvman.2026.128908.

Sadisun, I.A., Shimada, H., Ichinose, M., Matsui, K., 2002. Improved procedures for evaluating physical deterioration of argillaceous rocks. In: Proc. 2nd Intl. Conf. on New Development in RockMech. and Rock Eng, pp. 36–39. https://doi.org/10.13140/2.1.3499.8400.

Santo, A.P., Garzonio, C.A., Pecchioni, E., Salvatici, T., 2025. Petrophysical characterisation and suitability of serpentinites from the Monteferrato area (Tuscany, Italy) for architectural restoration. Minerals 15, 1105. https://doi.org/10.3390/min15111105.

Selen, L., Panthi, K.K., Vistnes, G., 2020. An analysis on the slaking and disintegration extent of weak rock mass of the water tunnels for hydropower project using modified slake durability test. Bull. Eng. Geol. Env. 79, 1919–1937. https://doi.org/10.1007/s10064-019-01656-2.

Singh, R., Fitzgerald, S., Dada, R., Frank, A.L., 2025. Marble waste dump yard in Rajasthan, India revealed as a potential asbestos exposure hazard. Int. J. Env. Res. Public Health 22, 215. https://doi.org/10.3390/ijerph22020215.

Taylor, A.R., Olsen, A.A., Hausrath, E.M., Olsen, B.J., Cardace, D., 2024. The role of sulfuric acid, abiotic–organic acids, and biotic acids on serpentinite dissolution and trace metal release. Minerals 14, 256. https://doi.org/10.3390/min14030256.

Ulusay, Hudson, 2007. The ISRM suggested methods for rock characterization, testing and monitoring: 2007-2014. Bull. Eng. Geol. Env. 74 (2015), 1499–1500. https://doi.org/10.1007/s10064-015-0780-3.

Valdelamar Martínez, D.E., Saba, M., Torres Gil, L.K., 2024. Assessment of asbestos-cement roof distribution and prioritized intervention approaches through hyperspectral imaging. Heliyon 10 (3). https://doi.org/10.1016/j.heliyon.2024.e25612.

Vergara, M.R., Triantafyllidis, T., 2016. Influence of water content on the mechanical properties of an argillaceous swelling rock. Rock Mech. Rock Eng. 49 (7), 2555–2568.

Vignaroli, G., Rossetti, F., Belardi, G., Billi, A., 2011. Linking rock fabric to fibrous mineralisation: a basic tool for the asbestos hazard. Nat. Hazards Earth Syst. Sci. 11, 1267–1280.

Viti, C., Mellini, M., 1997. Contrasting chemical compositions in associated lizardite and chrysotile in veins from Elba, Italy. Eur. J. Miner. 9, 585–596.

Viti, C., Mellini, M., 1998. Mesh textures and bastites in the Elba retrograde serpentinites. Eur. J. Miner. 10, 1341–1359.

Wong, L.N.Y., Maruvanchery, V., Liu, G., 2016. Water effects on rock strength and stiffness degradation. Acta Geotech. 11 (4), 713–737.

Yuhas, R.H., Goetz, A.F.H., Boardman, J.W., 1992. Discrimination among semi-arid, landscape endmembers using spectral angle mapper (SAM) algorithm Summaries of, the 4th Annual JPL Airborne Geoscience Workshop, JPL Pub-92-14, AVIRIS, Workshop. Jet. Propuls. Lab., Pasadena, CA, pp. 147–150.https://ntrs.nasa.gov/citations/19940012238.

Zholobenko, V., Rutten, F., Zholobenko, A., Holmes, A., 2021. In situ spectroscopic identification of the six types of asbestos. J. Hazard. Mater. 403, 123951. https://doi.org/10.1016/j.jhazmat.2020.123951. ISSN 0304-3894.